# Mechanical Properties of Bulk Nanocrystalline Aluminum-Tungsten Alloys

K.V. RAJULAPATI, R.O. SCATTERGOOD, K.L. MURTY, Z. HORITA, T.G. LANGDON, and C.C. KOCH

The Al-W alloy powders containing up to 4 at. pct W particles in a nanocrystalline Al matrix were synthesized by ball milling and then hot compacted (HC) at 573 K or cold compacted using high-pressure torsion (HPT). Hardness measurements were made to determine the effects on mechanical properties. Based on existing models, the hardening effect of W particles in HC samples was attributed to Orowan-particle strengthening. Composite-type strengthening due to large W particles appeared to be negligible. Both the compressive strain and shear strain in high pressure torsion added to the strengthening effects without producing a change in the grain size.

DOI: 10.1007/s11661-008-9593-3


## I. INTRODUCTION

A special class of advanced materials, nanocrystalline metals with grain size $<100$ nm, has triggered much activity among the scientific community in the past two decades because of their novel physical, chemical, and mechanical properties.[1] Refinement of the grain size to the nanoscale leads to a large enhancement of mechanical strength due to Hall–Petch (HP) strengthening, although there are some exceptions at smaller grain sizes.[2] Dispersions of second-phase particles can increase the strength of coarse-grained metals *via* Orowan strengthening or particulate-composite strengthening.[3] The effects of the size, spacing, and distribution of these particles on the mechanical properties of coarse-grained metals are well established.[4] However, the literature for strengthening effects due to second phases in nanocrystalline matrices is relatively sparse.[5] There are several reports on the development of multiphase bulk nanocrystalline aluminum alloys with high strength.[6] These materials were prepared by controlled crystallization of amorphous precursors. Hence, the second phase was either crystalline or quasi-crystalline depending on the crystallization kinetics and the material system. Often the problem associated with materials made by this method is the incomplete transformation of an amorphous matrix into a fully nanocrystalline structure.

Experimental and theoretical studies indicate that the deformation mechanisms for pure nanocrystalline metals are controlled by grain boundaries.[6–10] It was revealed with the aid of molecular dynamics simulations that mechanisms involving grain boundary sliding, grain rotation, and dislocation nucleation/absorption at grain boundaries become important at small grain sizes. Second phases dispersed in a nanocrystalline matrix are expected to influence the deformation mechanisms. The aim of the work reported here was to investigate the influence of a harder second phase, pure W, on the mechanical properties of a softer nanocrystalline Al matrix. Recent work has shown unusual softening effects for the complementary system of a soft second phase, pure Pb, in the harder nanocrystalline Al matrix.[11]

## II. EXPERIMENTAL PROCEDURE

The Al and W powders ($-325$ mesh) of purity greater than 99.9 pct were procured from Alfa-Aesar Inc., Ward Hill, MA. The powders were loaded into a tool steel vial in a glove box under a high-purity argon atmosphere ($<3$ ppm oxygen). Martensitic stainless steel balls (440C) were used as the milling media with a Spex 8000 (Metuchen, NJ) shaker mill. Initially, pure Al and Al + 1, 2, 3, and 4 at. pct W powders (0.96, 1.9, 2.9, and 3.8 vol pct W) were milled for 25 hours at room temperature.

In order to avoid cold welding between powder particles, 1.5 wt pct stearic acid was used as a surfactant. The resultant powders were consolidated into 6.35-mm-diameter disks by hot compaction at 573 K using a compressive stress of 1.8 GPa under an argon atmosphere. The density of the samples was measured using the Archimedes principle method. The hardness measurements were taken using a Buehler Micromet microhardness tester (Buehler Ltd., Lake Bluff, IL) at 100 g load. Before taking the hardness readings, samples were polished to a mirrorlike surface. The hardness

K.V. RAJULAPATI, Doctoral Student, formerly with the Department of Materials Science and Engineering, North Carolina State University, Raleigh, NC 27695-7907, is with the USC Andrew and Erna Viterbi School of Engineering, University of Southern California, Los Angeles, CA 90089-1453. Contact e-mail: rajulapa@usc.edu R.O. SCATTERGOOD, K.L. MURTY, and C.C. KOCH, Professors, are with the Department of Materials Science and Engineering, North Carolina State University. Z. HORITA, Professor, is with the Department of Materials Science and Engineering, Faculty of Engineering, Kyushu University, Fukuoka 819-0395, Japan. T.G. LANGDON, Professor, is with the Departments of Aerospace & Mechanical Engineering and Materials Science, University of Southern California.

Manuscript submitted June 12, 2007.
Article published online July 16, 2008

values reported are the average of 10 readings for each datum point.

In the second processing route, the as-milled nanocrystalline powders were cold compacted at room temperature into 0.8-mm-thick pellets of 10-mm diameter. These samples were then subjected to high-pressure torsion (HPT) at room temperature using facilities available at Kyushu University (Fukuoka, Japan).[12] The HPT processing was conducted under constrained conditions[13] using an imposed pressure of 2.5 GPa and 5 total revolutions of torsional shear at a rotation speed of 1 revolution per minute. Both the hot compacted (HC) and HPT samples were metallographically polished (to a mirrorlike surface finish) on different grit-sized SiC papers followed by fine polishing with 50-nm-sized alumina particle suspension. The microhardness measurements for the HPT samples were conducted at a load of 20 g (dwell time = 15 s). The HC and HPT samples were ≈98 pct and fully dense, respectively. X-ray diffraction (XRD) scans to determine the grain size and lattice strain were performed on a Rigaku Geigerflex diffractometer with Cu $K_\alpha$ radiation. The grain size and lattice strain for HPT samples were determined at various positions along the sample diameter using microfocus XRD scans (≈0.8-mm spot size) on a Bruker AXS D-5000 diffractometer (Madison, WI) with Cu $K_\alpha$ radiation. The grain sizes were computed using the Scherrer equation after accounting for instrumental broadening. The lattice strain was computed using the Stokes–Wilson formula. Samples for transmission electron microscopy were thinned with 20 pct perchloric acid and 80 pct methanol at 243 K using a Fischione (Export, PA) twin jet electropolisher and observed in a JEOL* 2010F transmission electron microscope (TEM) operated at 200 kV.

*JEOL is a trademark of Japan Electron Optics Ltd., Tokyo.

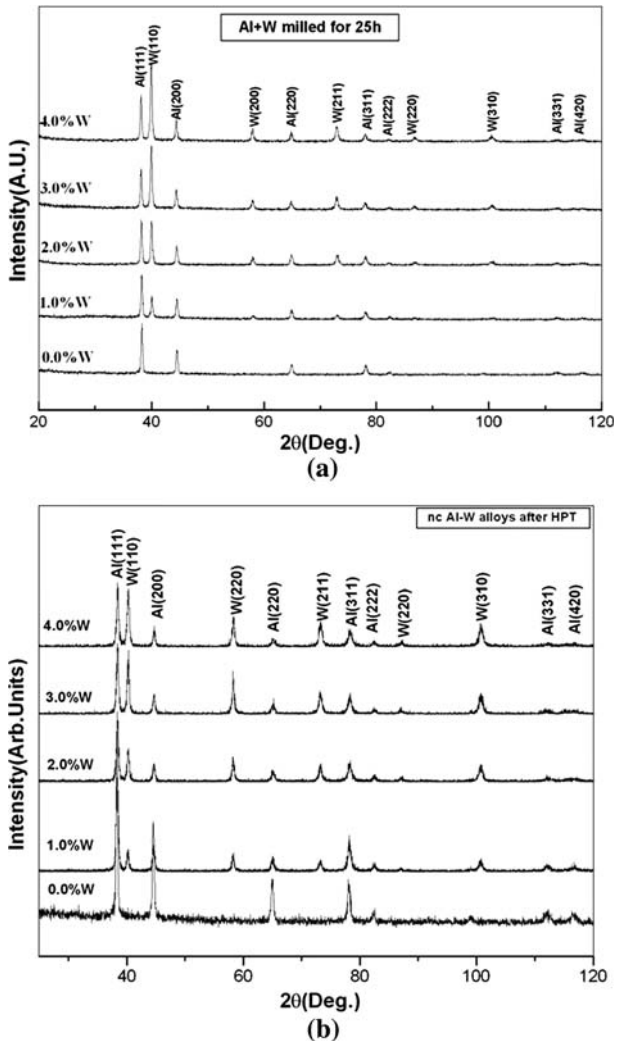


Fig. 1—XRD diffraction scans for the Al-W alloys: (*a*) as-milled and (*b*) after HPT processing.

## III. RESULTS AND DISCUSSION

Figures 1(a) and (b) show XRD scans for the as-milled alloys and the HPT-processed alloys, respectively. The scans indicate that only Al and W reflections are present, without the formation of intermediate phases. The grain size of Al was 29 ± 3 nm for as-milled Al and Al-W alloys. It increased to 34 ± 2 nm for HC Al and Al-W alloys. The W grain size was 34 ± 2 nm in both the as-milled Al-W and HC alloys. The Al and W grain sizes were 25 ± 3 and 27 ± 3 nm, respectively, in Al and the Al-W alloys after HPT processing. Microfocus XRD showed that the grain sizes remained uniform across the diameter of the HPT disks, where this is consistent with earlier results reported using X-ray microdiffraction with samples of pure Cu and a Cu-30 pct Zn alloy.[14] By contrast, the lattice strain for both Al and W varied across the disk diameter, as shown in Figure 2 ($r$ = 0 denotes the center). Precise lattice parameters of Al in Al-W alloys were estimated using the Nelson–Riley analysis.[15] The results gave $a_{Al}$ = 4.0445 ± 0.0020 Å compared to the standard lattice parameter $a_{Al}$ = 4.0494 Å. The difference is within the instrumental error, indicating that the ball milling and compaction routes produced two-phase mixtures of pure Al and W without formation of intermediate phases or metastable solid solutions.

High-energy ball milling and HPT are known to produce materials with a high density of lattice defects, grain boundaries, and triple junctions.[16,17] These defect regions act as high diffusivity pathways. There are many examples showing the formation of metastable compounds, intermediate phases, and metastable or supersaturated solid solutions in highly immiscible binary systems after high energy ball milling.[18] The equilibrium phase diagram of Al-W[19] shows the existence of three intermediate phases at low temperatures (< 500 °C). In spite of the high diffusivity pathways, the only phases observed in the Al-W alloys were the elemental metals. To the authors' knowledge, no previous studies of the ball milling of Al and W powders have been reported. Al-Mo is similar to Al-W and has been studied by Zdujic *et al.*[20] Even though the Al-Mo phase

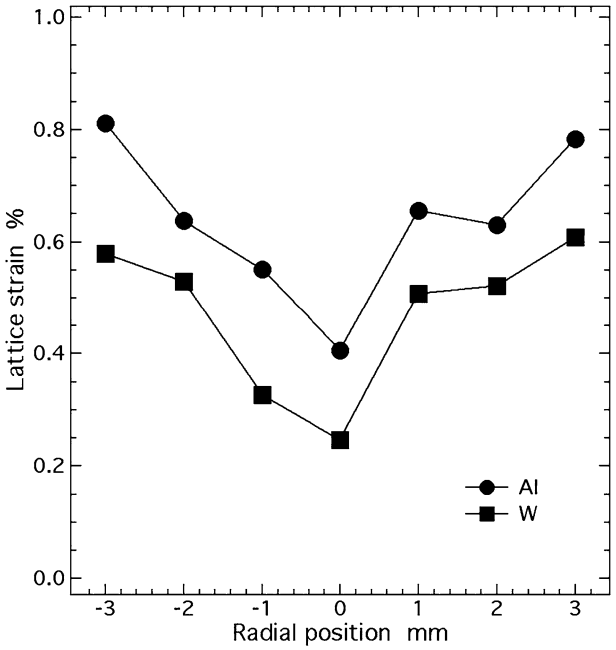


Fig. 2—Lattice (internal) strain for Al and W determined by micro-focus XRD at different radial positions across an HPT disk of Al-2 at. pct W.

diagram exhibits five intermediate phases, only elemental Al and Mo were observed after long milling times. The lattice parameter of Al in Al-rich Al-Mo alloys was observed to decrease with milling time, indicating the formation of a metastable solid solution of Mo in Al. Experimental measurements of the diffusion of Mo into Al have been reported.[21] The diffusivity is about an order of magnitude less than for the diffusion of Ni in Al at 400 °C. Although no data on diffusion of W in Al has been found, it can be assumed that low diffusivities exist in this system. The self-diffusivity of Mo at 1800 °C is about $10^4$ greater than for W at this temperature. The extrapolated self-diffusivity for W to the upper limit for milling temperatures (<400 °C) gives extremely low values. It follows that the diffusivity of W in Al should be negligible during milling, to the extent that the presence of a high concentration of vacancies and dislocations does not facilitate the formation of intermediate phases or metastable solid solutions.

Figures 3(a) and (b) show typical dark-field and bright-field TEM micrographs, respectively, for the Al-W microstructures. Figure 3(c) is a diffraction pattern corresponding to Figure 3(a). Indexing of the rings revealed a superposition of polycrystalline diffraction patterns for pure Al and pure W. Figure 3(b) shows the typical distribution of W particles (dark) at lower magnification. The TEM grain size was larger than the XRD grain size by about 10 pct. The XRD values are used for comparison, because TEM grain-size distributions were limited to a few cases.

Figure 4 shows the hardness of the HC Al-W alloys as a function of the volume fraction of W. The data show an upward trend as the volume percent of W increases. W-particle strengthening of the nanocrystalline Al matrix could be a result of a composite strengthening effect due to W particles larger than the Al matrix grain size or an Orowan dislocation-particle strengthening effect for smaller W nanoparticles contained within Al grains. The distribution of the W-particle sizes seen in Figure 3(b) was not characterized quantitatively. It ranges in size from less than the Al-matrix grain size up to particle sizes in excess of 500 nm.

Rule-of-mixture relations are often used to describe composite properties. They are conveniently independent of all microstructure strength-related parameters, except for the hardness of the particles and matrix. The matrix hardness in the HC Al-W alloys is the same as pure Al (0.934 GPa), because the Al grain size is constant at $d_{Al} = 34$ nm. The grain size of W was $d_W = 34$ nm and remained constant in the alloys. The hardness of the W particles is not known. Pure W was ball milled and HC, producing bulk W with a hardness of 14.2 GPa and a 6-nm grain size. To compensate for the grain size difference, a model recently developed for grain size HP strengthening and Orowan particle strengthening in nanocrystalline alloys[22] will be used here; suitable hardness *vs* grain size data for pure nanocrystalline W was not found in the literature. The model equations are

$$H_{HP} = H_o + \frac{3G\mathbf{b}}{\pi}\frac{1}{d}\ln\frac{d}{r_o} \quad [1]$$

$$\Delta H_p = \frac{3G\mathbf{b}}{\pi}\left\{\frac{1}{d(1-\sqrt{f})}\left[\frac{d\sqrt{f}}{D}\ln\frac{D}{r_o} + \ln d\right] - \frac{1}{d}\ln\frac{d}{r_o}\right\} \quad [2]$$

where $H_{HP}$ in Eq. [1] is the hardening due to grain size $d$, *i.e.*, the HP effect; $r_o$ is the core-cutoff distance in the dislocation line energy; $D$ is the size of W particles; $G$ is the shear modulus; $\mathbf{b}$ is the Burgers vector; and $H_o$ is a free parameter. The term $\Delta H_p$ in Eq. [2] is the Orowan-hardening increment for a volume fraction $f$ of second-phase particles with diameter $D < d$. An inverse square-root relation for $d$ is not obtained in Eq. [1]. On a conventional HP plot, the logarithm term will produce a decreasing slope with decreasing $d$ and an inverse HP effect at very small $d$ values. Equation [1] can be approximated by $d^{-1/2}$ behavior over restricted ranges of $d$ values,[22] but that is not needed to obtain an estimate of the hardness of W with grain size $d_W = 34$ nm. Using the values $r_o = 1$ nm, $G = 161$ GPa, and $\mathbf{b} = 0.274$ nm in Eq. [1] with the measured values $H_W = 14.2$ GPa at $d_W = 6$ nm, we obtain $H_o = 1.6$ GPa. Back calculating using this $H_o$ value gives $H_W = 5.9$ GPa at $d_W = 34$ nm. We take this to be the effective hardness for large polycrystalline W particles, $D > d_{Al}$, that would contribute to composite strengthening. Smaller particles would contribute to Orowan strengthening.

Rule-of-mixtures, $H_{AlW} = (1-f)H_{Al} + fH_W$, and inverse rule-of-mixtures, $1/H_{AlW} = (1-f)/H_{Al} + f/H_W$, lines are shown in Figure 4. These were obtained using $H_{Al} = 0.934$ GPa and $H_W = 5.9$ GPa. It is assumed that W is present only as large particles $D > d_{Al}$. The

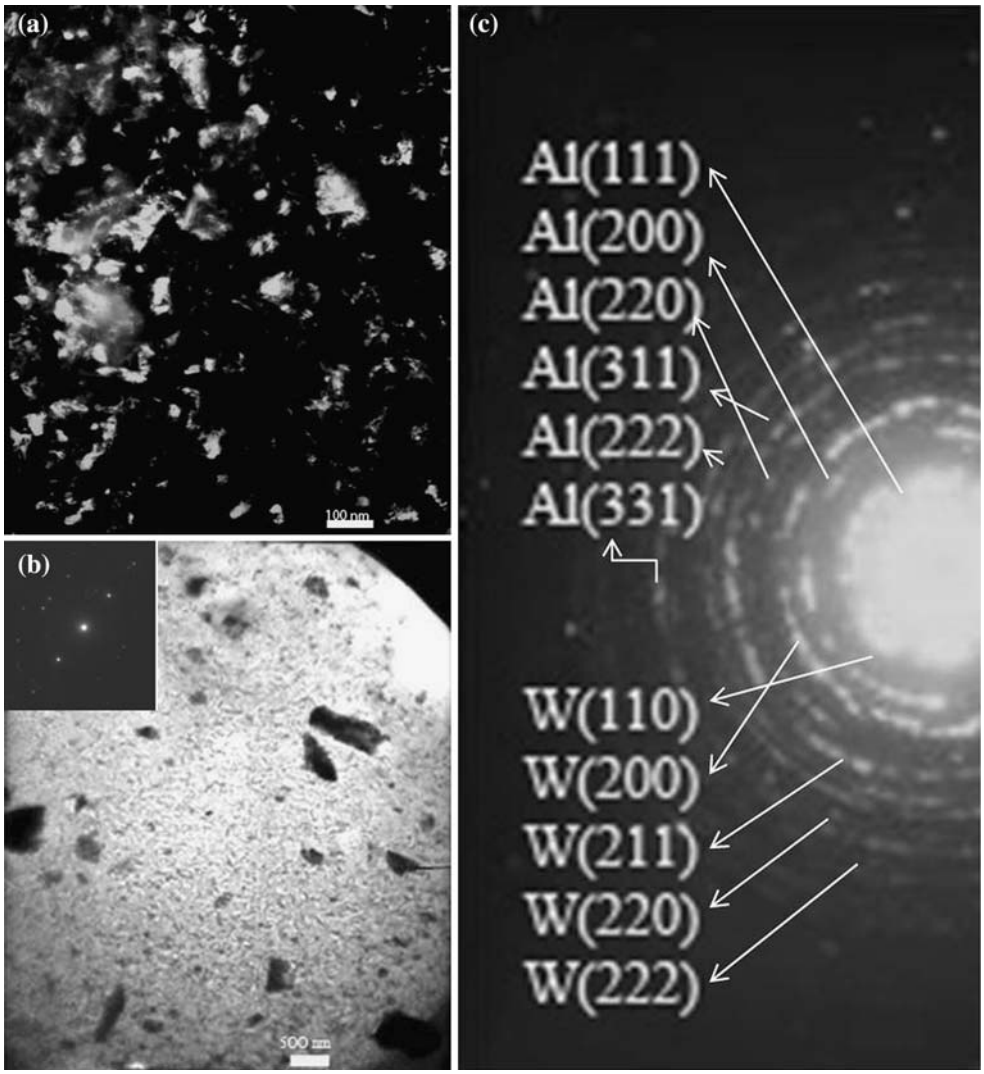


Fig. 3—TEM results for the HPT Al-2 at. pct W alloy. Results for other HPT and HC alloys are similar. (*a*) TEM dark-field image showing the Al grains. Al (111) ring was used in obtaining this dark-field image. (*b*) Bright-field TEM showing the W particle size distribution. The diffraction pattern in the inset is from one of the bigger W particles. (*c*) Diffraction pattern corresponding to (a).

initial hardening rate in Figure 4 follows close to the rule-of-mixtures line (dashed). Above 2 vol pct W, the increase is faster. This is in contrast to the embedded-cell[23] and finite-element simulations[24] for particle-reinforced matrices. These models predict very low hardening rates at smaller particle volume fractions $f < 0.2$.[23] In fact, the predictions for hard deformable particles[24] follow close to the inverse rule-of-mixtures line (solid) in Figure 4. This effect has been observed experimentally, for example, with Ni particles in Ag-Ni alloys.[23,24] If hard W particles in the nanocrystalline Al-W alloys produce composite strengthening, it appears to differ from that expected/observed in similar, conventional grain-size alloys. The features unique to a nanocrystalline microstructure that would give rise to a new mechanism are not evident. Accordingly, there is no reason to conclude that the initial agreement of the data points in Figure 4 with the rule-of-mixtures line is the manifestation of a nanoscale composite strengthening mechanism; the agreement is considered to be fortuitous.

Orowan strengthening due to dislocation-particle interaction is possible when $D < d_{Al}$. Assuming that the Orowan hardening increment $\Delta H_p$ superimposes linearly with the Al matrix hardness $H_{Al}$, Eq. [2] can be used to predict the Al-W alloy hardness as a function of vol pct W. Figure 5 shows the results for a range of $D$ values from 5 to 25 nm, using $G = 26.1$ GPa, $\mathbf{b} = 0.286$ nm, $d_{Al} = 34$ nm, and $H_{Al} = 0.934$ GPa for the Al matrix. In the calculations for each size $D$, it is assumed that all of the W consists of particles of that size. These results clearly establish that Orowan hardening is more than sufficient to account for the strengthening effect. Furthermore, it is only necessary that a fraction of the total volume of W particles is in a size range $D < d_{Al}$ to account for the overall magnitude of the strengthening. For example, the curve labeled D15 at 30 pct in Figure 5 shows the result when 30 pct of the total volume of W has a particle size $D = 15$ nm and the remaining particles are inert.

The trend does not match that of the HC data points in this case. However, for the span of the Orowan curves

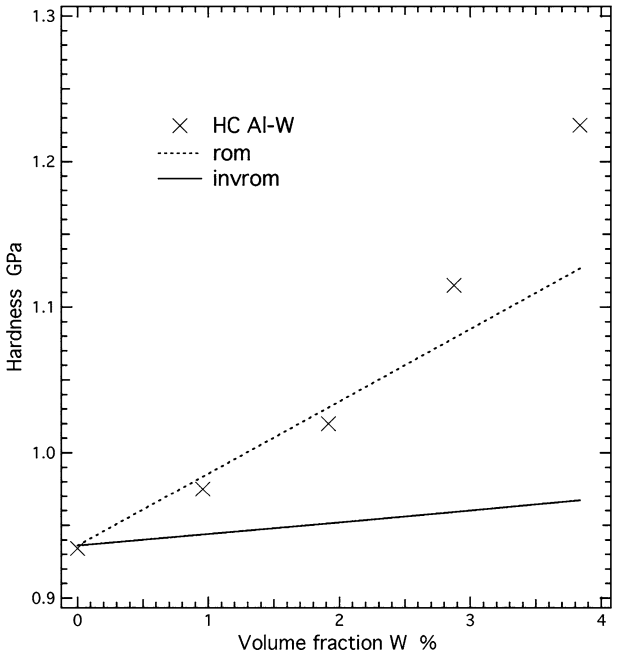


Fig. 4—Hardness *vs* vol pct W curve for the HC alloys. Rule-of-mixtures (rom) and inverse rule-of-mixtures (invrom) lines are shown.

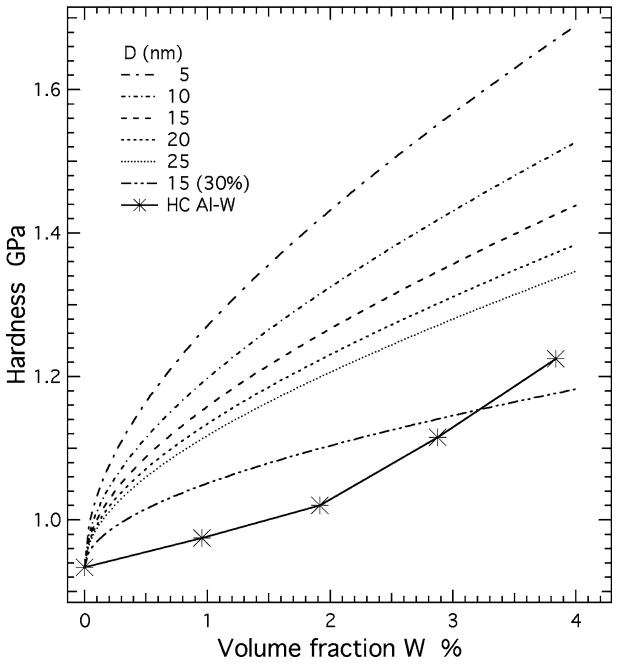


Fig. 5—Hardness *vs* vol pct W curves obtained using Eq. [2], as described in the text. The HC data points from Fig. 4 are shown.

for different $D$ values in Figure 5, one can "deconvolute" a relative amount and size distribution of particles $D < d_{Al}$ to match the HC data points over the range of vol pct W. The remaining W particles with $D > d_{Al}$ would, according to the composite model predictions discussed previously, contribute only marginally to the hardening effect. This analysis is not presented, because we do not have experimental data for the W-particle size distributions for comparison.

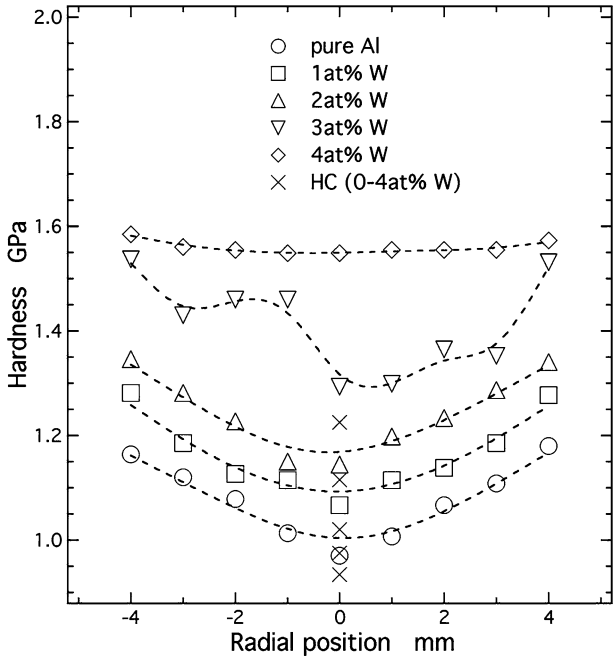


Fig. 6—Hardness *vs* radial position curves for the HPT alloys. The HC data points from Fig. 4 are shown at $r = 0$. Dashed lines are the trends obtained from an interpolation fit.

Figure 6 shows the hardness obtained for the Al-W alloys after HPT processing. The hardness is shown as a function of the radial position $r$ across a diameter of the $h = 0.8$-mm-thick disks ($r = 0$ denotes the center position with respect to $\pm r$ changes). The trends remained consistent for different angular positions of the diameter, except for 3 at. pct W, where noncentrosymmetric variations are present. The HPT process produces both compression and shear. In the ideal case, the compression strain remains uniform and the torsion shear strain will vary from 0 at the center position to $\theta r/h \approx 160$ at $r = \pm 4$ mm after 5 revolutions. An equivalent von Mises shear strain can also be used to characterize HPT shear deformation,[25] and this would be ~5 at $r = \pm 4$ mm. Additional hardening due to shear strain is reflected by the upward trend in the curves as a function of $\pm r$. Because the Al matrix grain size remained constant over the disk diameter, the increase in hardness for pure Al may be the result of strain hardening/twinning effects in the nanoscale grain structure. There is a relatively constant upward shift in the curves in Figure 6 for 0 to 2 pct W. At 3 pct W, there is fluctuating transition behavior that leads to a relatively flat curve at 4 pct W. The trend of increasing hardness near the edges of the HPT disks is consistent with a wide range of data covering several different materials.[12,13,26–28] However, it should be noted that for pure Al, where the stacking fault energy is very high and there is a rapid rate of recovery, the measured hardness is higher in the central region of the disk after a single turn but gradually becomes more equilibrated after increasing numbers of turns.[29]

Figure 6 also shows the hardness data for the HC-processed alloys, plotted at the $r = 0$ position.

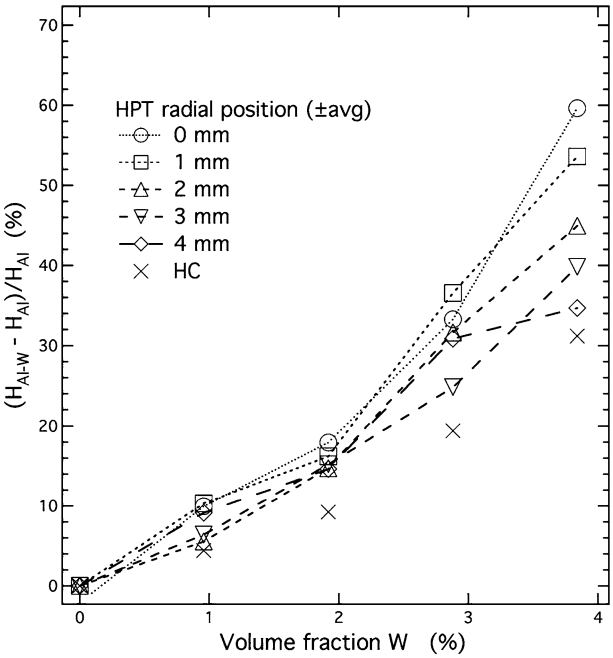


Fig. 7—Relative percentage changes in the hardness *vs* vol pct W for different radial positions. The results are the $\pm r$ average values from Fig. 6. The HC data points from Fig. 4 are shown.

The change in hardness with pct W in the HPT alloys at $r = 0$ is significantly larger than in the HC alloys. A smaller Al-matrix grain size in HPT (25 nm) *vs* HC (34 nm) alloys will account for about 15 pct of this increase. The remaining differences are due to HPT straining effects at the $r = 0$ position.

Figure 7 shows the results in Figure 6 plotted as a percentage increase of the Al matrix hardness. The values shown are the $\pm r$ averages from Figure 6. The hardness-change curves for the HPT alloys become less steep as $r$ increases. They approach the HC curve, but still lie above it. As the shear strain increases with $r$, the relative hardness change due to HPT processing appears to saturate near the HC result. This implies that the effect of large HPT shear strain on the W particles scales proportional with its effect on the pure Al matrix. This could result, for example, if a geometrically necessary dislocation accumulation around W particles (producing internal strain within them) scales with dislocation accumulation in the matrix/grain boundaries. The internal strains in the Al matrix and in W particles in Figure 2 show comparable trends that would at least be consistent with a scaling assumption.

## IV. SUMMARY AND CONCLUSIONS

Nanocrystalline Al-W alloy powders containing pure Al with second-phase pure W particles were synthesized by ball milling. Samples were HC at 573 K and cold compacted using HPT. The effect of W additions on HC Al-W alloys produced a maximum hardening effect on the order of 30 pct. It was concluded that Orowan hardening due to W particles within Al grains was the dominant mechanism. It was further proposed that a range of particle sizes must be in the overall distribution that accounts for the hardening trend observed. Based on rule-of-mixtures models for conventional (large grain size) particle-reinforced alloys, the W particles larger than the matrix grain size do not appear to be effective in producing hardening. Cold-compacted nanocrystalline Al-W disk samples were further processed by HPT. Additional grain-size-independent strengthening due to both compressive strain and torsional shear strain was manifested from the change in hardness as a function of radial position on the disks. At large shear strains, there appears to be saturation in the relative change in hardness with vol pct W. This was attributed to a scaling of dislocation accumulation around particles with that in the matrix/grain boundaries.

## ACKNOWLEDGMENTS

This research was supported by the United States National Science Foundation under Grant No. DMR-0201474. This work is also supported, in part, by a Grant-in-Aid for Scientific Research on Priority Areas, from the Ministry of Education, Culture, Sports, Science and Technology, Japan.

## REFERENCES

1. C.C. Koch: *Nanostructured Materials: Processing, Properties and Applications*, Noyes Publishing/William Andrew Publishing, Norwich, NY, 2002.
2. M.A. Meyers, A. Mishra, and D.J. Benson: *Progr. Mater. Sci.*, 2006, vol. 51, pp. 427–56.
3. G.E. Dieter: *Mechanical Metallurgy*, 3rd ed., McGraw-Hill, Boston, MA, 1986, p. 184.
4. M.A. Meyers and K.K. Chawla: *Mechanical Behavior of Materials*, Prentice-Hall, Upper Saddle River, NJ, 1999, p. 484.
5. Z. Horita, K. Ohashi, T. Fujita, K. Kaneko, and T.G. Langdon: *Adv. Mater.*, 2005, vol. 17, pp. 1599–1602.
6. F. Schurack, J. Eckert, and L. Schultz: *Nanostruct. Mater.*, 1999, vol. 12, pp. 107–10.
7. K.S. Kumar, H. Van Swygenhoven, and S. Suresh: *Acta Mater.*, 2003, vol. 51, pp. 5743–74.
8. V. Yamakov, D. Wolf, S.R. Phillpot, A.K. Mukherjee, and H. Gleiter: *Nat. Mater*, 2004, vol. 3, pp. 43–47.
9. D. Wolf, V. Yamakov, S.R. Phillpot, A.K. Mukherjee, and H. Gleiter: *Acta Mater.*, 2005, vol. 53, pp. 1–40.
10. H. Van Swygenhoven and J.R. Weertman: *Mater. Today*, 2006, vol. 9, pp. 24–31.
11. K.V. Rajulapati, R.O. Scattergood, K.L. Murty, G. Duscher, and C.C. Koch: *Scripta Mater.*, 2006, vol. 55, pp. 155–58.
12. G. Sakai, Z. Horita, and T.G. Langdon: *Mater. Sci. Eng. A*, 2005, vol. 393, pp. 344–51.
13. A.P. Zhilyaev, K. Oh-ishi, T.G. Langdon, and T.R. McNelley: *Mater. Sci. Eng. A*, 2005, vols. 410–411, pp. 277–80.
14. T. Ungár, L. Balogh, Y.T. Zhu, Z. Horita, C. Xu, and T.G. Langdon: *Mater. Sci. Eng. A*, 2007, vol. 444, pp. 153–56.
15. B.D. Cullity: *Elements of X ray Diffraction*, 3rd ed., Addison-Wesley, New York, NY, 1978, p. 330.
16. G. Palumbo, S.J. Thorpe, and K.T. Aust: *Scripta Metall. Mater.*, 1990, vol. 24, pp. 1347–50.
17. B.B. Straumal, B. Baretzky, A.A. Mazilkin, F. Phillip, O.A. Kogtenkova, M.N. Volkov, and R.Z. Valiev: *Acta Mater.*, 2004, vol. 52, pp. 4469–78.
18. C. Suryanarayana: *Mechanical Alloying and Milling*, CRC Press Publications, Boca Raton, FL, 2004.

19. H. Okamoto: *Desk Handbook, Phase Diagrams for Binary Alloys*, ASM INTERNATIONAL, Materials Park, OH, 2000, p. 48.
20. M.V. Zdujic, K.F. Kobayashi, and P.H. Shingu: *J. Mater. Sci.*, 1991, vol. 26, pp. 5502–08.
21. A.R. Paul and R.P. Agarwala: *J. Appl. Phys.*, 1967, vol. 38, pp. 3790–91.
22. R.O. Scattergood, C.C. Koch, K.L. Murty, and D. Brenner: *Mater. Sci. Eng. A*, 2007, in press.
23. M. Dong and S. Schmauder: *Acta Mater.*, 1996, vol. 44, pp. 2465–78.
24. H.S. Kim: *Mater. Sci. Eng. A*, 2000, vol. 289, pp. 30–33.
25. A.P. Zhilyaev, T.R. McNelley, and T.G. Langdon: *J. Mater. Sci.*, 2007, vol. 42, pp. 1517–28.
26. H. Jiang, Y.T. Zhu, D.P. Butt, I.V. Alexandrov, and T.C. Lowe: *Mater. Sci. Eng. A*, 2000, vol. 290, pp. 128–38.
27. A.P. Zhilyaev, G.V. Nurislamova, B.K. Kim, M.D. Baró, J.A. Szpunar, and T.G. Langdon: *Acta Mater.*, 2003, vol. 51, pp. 753–65.
28. A. Vorhauer and R. Pippan: *Scripta Mater.*, 2004, vol. 51, pp. 921–25.
29. C. Xu, Z. Horita, and T.G. Langdon: *Acta Mater.*, 2007, vol. 55, pp. 203–12.